Express Polymer Letters Vol.17, No.8 (2023) 850–866
Available online at www.expresspolymlett.com
https://doi.org/10.3144/expresspolymlett.2023.63

Research article

Mechanical/electrical properties and strain sensibility of epoxidized natural rubber nanocomposite filled with carbon nanotube: Effect of sodium alginate as a surfactant on latex technology process

Apinya Krainoi[1], *Kanoktip Boonkerd*[1,2*]

[1]Department of Materials Science, Faculty of Science, Chulalongkorn University, Thailand
[2]Center of Excellence in Green Materials for Industrial Application, Chulalongkorn University, Thailand

Received 15 February 2023; accepted in revised form 27 April 2023

Abstract. This study focused on the role of sodium alginate (Alg) as a surfactant in the mechanical/electrical properties and strain sensibility of carbon nanotube (CNT)-filled epoxidized natural rubber (ENR) nanocomposite. The preparation of ENR nanocomposite was carried out by a latex mixing process. CNTs were pre-treated with a dispersing agent and added to the ENR latex. To enhance the mechanical and electrical properties of nanocomposites for application as a strain sensor, we performed the homogenization of ENR/CNT suspension and fine dispersion of CNT in the ENR matrix. The effect of Alg on the properties of nanocomposites was estimated and compared with that of a common latex surfactant, that is, sodium dodecyl sulphate. The mechanical, electrical properties and strain sensitivity of ENR nanocomposites were improved with the use of Alg. In addition, the ENR nanocomposite films from latex technology mixing can be used in strain sensor applications, such as those with finger motion sensitivity.

Keywords: *nanocomposites, rubber, biopolymers, carbon nanotubes, strain sensibility*

1. Introduction

To date, carbon nanotube (CNT)-based polymer composites are widely studied as a realistic alternative to conventional smart materials as conducting polymers owing to their superior electrical properties [1]. The remarkable properties of polymer/CNT nanocomposites result in multifunctional properties, such as sensing and actuating capabilities. The research on stretchable and flexible sensors is attracting attention due to their numerous applications in wearable electronics, soft robotics, and remote health monitoring [2]. In addition, polymer/CNT nanocomposite flexible sensors can be used for long periods, are reliable, and compatible with industrial requirements [2] due to their high tensile strength, mechanical robustness, and low buckling of CNT/polymer nanocomposite. Several types of polymers have been used as the matrix of CNT-based nanocomposites for strain sensor applications; such nanocomposites include epoxy/CNT [1], polymethyl methacrylate (PMMA)/CNT [3], polycarbonate/CNT [4], polyelectrolyte/CNT [5], polyurethane/CNT [6], silicon rubber/CNT [2], and biopolymers including natural rubber (NR) (*Hevea brasiliensis*)/CNT composites [7, 8].

NR nanocomposites have earned considerable attention in this field not only because they are naturally based nanocomposites but also due to their high extensibility. NR itself offers superior elasticity, flexibility, and abrasion resistance, which can support the stretching capability of strain sensor applications.

*Corresponding author, e-mail: kanoktip.b@chula.ac.th

CNT-filled NR offered a strong strain-dependent characteristic in the 100 to 150% regime elongation [8]. Furthermore, alternative NR matrices were studied, and the results revealed that epoxidized NR (ENR) nanocomposites exhibited better mechanical properties than NR nanocomposites, which helped recover resistivity to the original value after 20 extension cycles of ENR nanocomposites [7]. The chemical linkages in the ENR nanocomposites were primarily responsible for this finding.

Moreover, the processing of CNT-based NR nanocomposites enhances mechanical and electrical properties from the aspect of CNT dispersion in the NR matrix. Most of rubber nanocomposites are produced through a melt-blending mixing process that employs an internal mixer and a two-roll mill [7, 8]. NR can be processed in different ways from various forms of raw materials, such as dried NR (*i.e.*, rubber sheet and rubber block), which is proper for the melt blending mixing process, and NR latex, which is apt for the latex mixing or latex technology process. However, mixing nano-sized fillers as CNTs into a high-viscosity NR matrix with a melt mixing process leads to inhomogeneous mixtures or the presence of agglomerated fillers [9]; thus, latex technology may be used to solve this problem.

The latex technology is a two-pot system using latex (first pot) and a nanoparticle–suspension (second pot) [9]. The use of water as a processing medium and minimal energy requirement makes the latex technology process environmentally friendly. Furthermore, the process is applicable to various fillers and polymers (latex state) [9]. In addition, CNT dispersion in the medium of water-filled NR latex improved the tensile properties and electrical conductivity of CNT-filled NR composites [10]. To achieve the fine dispersion of CNTs in NR, scientists should develop a stabilizer of aqueous CNT dispersion using a surfactant or dispersing agent before the addition of CNTs to the NR latex. Sodium dodecyl sulphate (SDS) is an important anionic surfactant that has hydrophilicity and hydrophobicity. The SDS surfactant in latex mixing of CNTs and NR resulted in the formation of infinite three-dimensional CNT networks in the NR matrix, which enhanced the electrical properties [11]. SDS increased the electrical conductivity of conductive NR composites, and the decrease in maximum stress can be attributed to the nanocomposite with a high SDS content, which resulted in the SDS domains as areas of stress concentration in the nanocomposite film [12]. Hence, scientists face the challenge of improving filler dispersion with the surfactant playing a role in enhancing electrical and mechanical properties of NR composites. The literature revealed the use of sodium alginate (Alg), which is a natural and non-toxic product, as a dispersing agent in the NR latex. The use of Alg improved the mechanical properties of NR composites [13]. Sodium Alg is the sodium salt of alginic acid, which is obtained from the cell wall component of marine brown algae, which contains approximately 30 to 60% alginic acid. The conversion of alginic acid to sodium Alg allows its dissolution in water [14]. Chemically, sodium Alg is a linear copolymer consisting mainly of residues of β-(1-4)-linked D-mannuronic acid and α-(1-4)-linked L-glucuronic acid units [15]. It has unique colloidal properties, such as thickening, stabilizing, suspending, film-forming, gel-producing, and emulsion-stabilizing properties [16, 17].

Therefore, this work proposed sodium Alg as a novel surfactant for the preparation of the ENR/CNT nanocomposite by a latex technology mixing process. The performance of Alg was evaluated comparatively with that of SDS. The properties related to strain sensor application, such as mechanical and electrical properties and piezoresistivity, were investigated.

2. Experimental

2.1. Materials

Natural rubber latex with 25% epoxidation (ENR25) was used in this study. The dispersing agents, such as sodium alginate (Alg) and sodium dodecyl sulphate (SDS), were purchased from Loba Chemie Pvt. Co., Ltd. (Mumbai, India) and Kemaus, Elago Enterprises Pty Ltd. (Cherrybrook, Australia), respectively. The multi-walled CNTs (NC7000) measured 9.5 nm in diameter and 1.5 μm in length, had 90% purity, and was manufactured by Nanocyl S.A. (Sambreville, Belgium). In addition, potassium hydroxide was manufactured by Qingdao Hisea Chem Co. Ltd (Qingdao, China). Potassium laurate, 50% zinc diethyldithiocarbamate, 50% poly(dicyclopentadiene-co-p-cresol), and 50% sulfur were supplied by Lucky Four Co., Ltd (Nonthaburi, Thailand).

2.2. Preparation of ENR nanocomposite vulcanizate films filled with CNT

The ENR/CNT nanocomposites were prepared by the latex technology mixing process. First, the

Table 1. Formulation for ENR latex compound.

Ingredients	Contents [phr]
40% ENR latex	100.00
20% Potassium Laurate (aqueous solution)	1.00
10% Potassium hydroxide (aqueous solution)	0.25
50% Zinc diethyldithiocarbamate dispersion	1.25
50% Poly(dicyclopentadiene-*co*-*p*-cresol) dispersion	1.00
50% Sulfur dispersion	2.00
50% ZnO dispersion	3.00

pre-vulcanized ENR latex was prepared following the formulation shown in Table 1. The compounding process was started by the addition of the chemical dispersion in Table 1 to the ENR latex. The mixture was mixed by mechanical stirring at 150 rpm with an overhead stirrer at room temperature for 24 h. Figure 1a reveals the so-called maturation of the pre-vulcanized ENR latex. Subsequently, the CNT dispersion was prepared (Figure 1b). Various types of surfactants (*i.e.*, SDS with 0.5% and Alg with 0.5% and 1% of ENR) were carefully dissolved in deionized (DI) water. The amount of water was related to the dilution of ENR latex from 40 to 20% dry rubber content. Moreover, 5 phr CNT by weight of 100 phr ENR content was dispersed in deionized water. The CNT suspension was then homogenized for 30 min by a high-speed homogenizer (FSH-2A, BELLAXX, Douai, France). Figure 1c reveals the preparation process of ENR/CNT nanocomposite films. The CNT dispersion was eventually added to the pre-vulcanized ENR latex and stirred by a magnetic stirrer for 10 min. The mixture was then cast on a glass plate and dried at 60 °C for 24 h. Finally, the ENR/CNT nanocomposite film was obtained. The ENR nanocomposite without the surfactant was labeled as ENR/CNT, and those added with 0.5% SDS and Alg were labeled as ENR/CNT-SDS and ENR/CNT-$Alg_{0.5}$, respectively. In addition, the ENR nanocomposite containing 1% Alg was denoted as ENR/CNT-Alg_1.

3. Characterizations

3.1. Attenuated total reflection Fourier-transform infrared spectroscopy (ATR-FTIR)

ATR-FTIR was used to examine the gum ENR, ENR/CNT, ENR/CNT-SDS, ENR/CNT-$Alg_{0.5}$, and

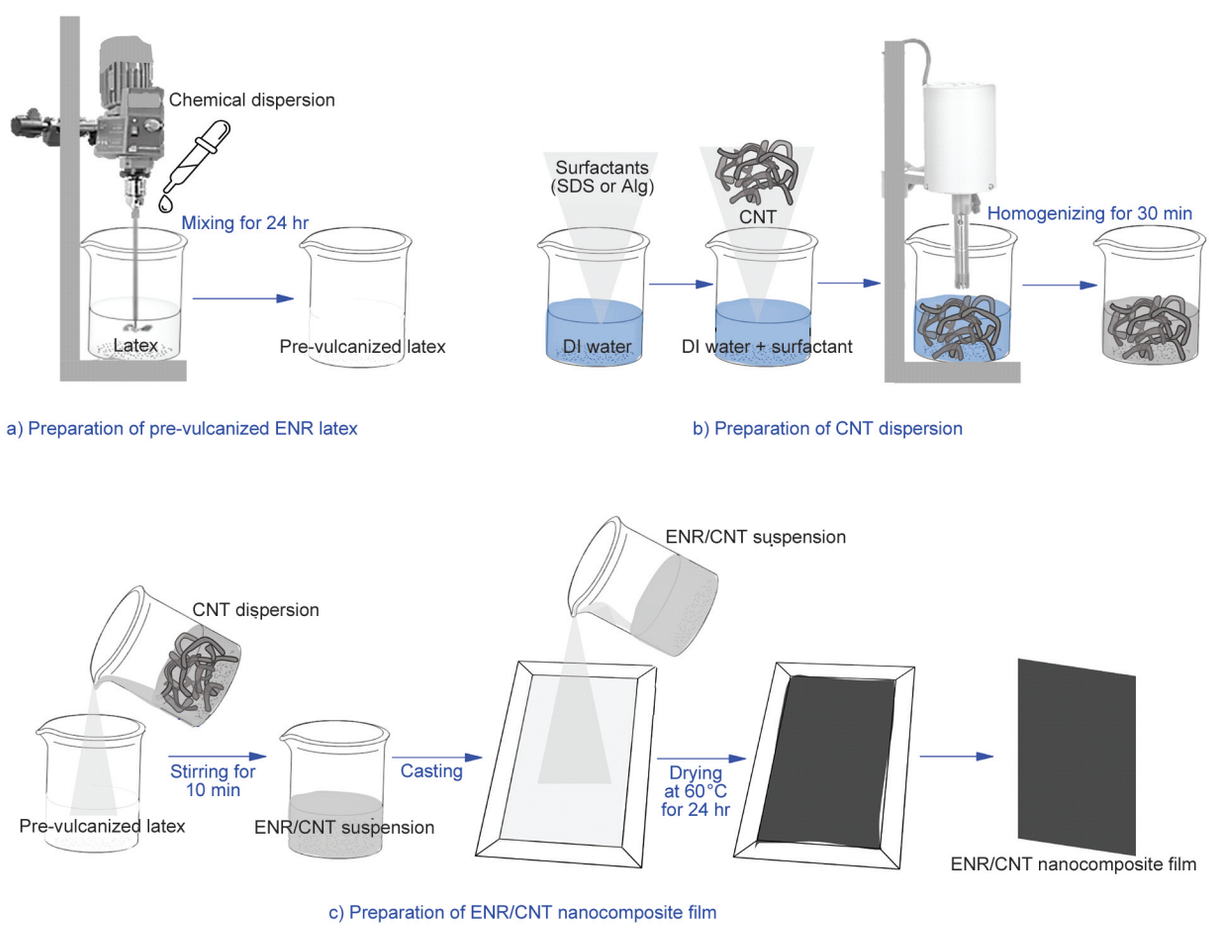

Figure 1. The preparation of pre-vulcanized ENR latex (a), CNT dispersion (b) and ENR/CNT nanocomposite films (c).

ENR/CNT-Alg_1 nanocomposites (Thermo Nicolet Avatar 360 FTIR, Thermo Electron Corporation, Thermo Nicolet, Madison, WI, USA). The analysis was carried out with a resolution of 4 cm^{-1} over a wide wavenumber range of 4000–600 cm^{-1}.

3.2. Mechanical properties

A universal tensile testing machine with a series dual-column table (Tinius Olsen, Co., Ltd., Honey Crock Lane, UK) was used to test the mechanical properties of gum ENR and ENR nanocomposite films with various surfactants. ISO 37 was used to prepare the dumbbell samples (type 5A). Testing was performed at room temperature with a crosshead speed of 500 mm/min. Furthermore, the hysteresis energy loss of ENR nanocomposites was evaluated by cyclically deforming the dumbbell specimen with various strains applied at 50, 100, and 300%.

3.3. Crosslink density

The crosslink densities of the samples were examined using the swelling method. The samples were weighed before being immersed in toluene for seven days at room temperature. The swollen weight was recorded after the swollen samples were taken out from the toluene. The swollen samples were then dried in a hot-air oven at 60 °C for another 24 hours after being evaporated at room temperature for 24 hours. Finally, the final weights of the dried samples were recorded. The Flory-Rehner Equation (1) was used to determine the apparent crosslink density [18]:

$$v = \frac{-\left(\ln\left(1-\phi_\rho\right)+\phi_\rho+\chi\phi_\rho^2\right)}{V_1\left(\phi_\rho^{1/3}-\frac{\phi_\rho}{2}\right)} \quad (1)$$

where v is the crosslink density [mol/m^3], ϕ_ρ is the volume fraction of rubber in a swollen network, V_1 implies to the molar volume of toluene [19]. In addition, χ is the Flory–Huggins interaction parameter between toluene and rubber, where a value of 0.376 was used for χ in accordance with the literature [20].

3.4. Dynamic mechanical thermal analysis (DMTA)

DMTA was performed in tension mode with DMTA-V (Rheometric Scientific, NJ). The samples were scanned over a temperature range of –80 to 60 °C at a heating rate of 3 °C/min and a fixed deformation frequency of 10 Hz.

3.5 Electrical properties

At room temperature, the electrical conductivities of gum ENR and all nanocomposites were measured using an inductance capacitance resistance meter (LCR meter) (Hioki IM 3533, Hioki E.E. Corporation, Nagano, Japan). The LCR meter was connected to the electrode plates. Sample was sandwiched between the electrode plates. The test was then carried out over a frequency range of 20–10^5 Hz. Electrical conductivity (σ) and dielectric constant (ε') were evaluated using Equations (2) and (3) [21, 22]:

$$\sigma = \frac{1}{\rho} = \frac{d}{R_p \cdot A} \quad (2)$$

$$\varepsilon' = \frac{C_p \cdot d}{A \cdot \varepsilon_0} \quad (3)$$

where ε_0 is the dielectric constant of free space, which is $8.854 \cdot 10^{-12}$ F/m. The symbols d and A refer to the sample thickness and area of an electrode, respectively. Factor ρ is the volume resistivity, that is, the reciprocal of conductivity. Moreover, R_p and C_p are resistance and capacitance, respectively.

The change in resistance ($\Delta R/R_0$) of ENR/CNT nanocomposites with various surfactants was measured using an in-house fabricated strain application instrument, The EYSIGHT B2901 (Keysight Technologies, California, USA) was used to detect the resistance. Dumbbell-shaped samples (ISO 527 type 5A) were prepared and clamped to the sample holder. To detect the relative resistance of the composites in each cycle, the samples were sequentially extended to 100% strain and released the force during cycling for 250 s at 50 mm/s of a crosshead speed.

3.6. Morphological property

The morphologies of ENR nanocomposite films were verified. To observe the cross-section surface of the samples, we first cryogenically fractured each specimen in liquid nitrogen. Subsequently, the samples were sputter-coated with a thin layer of gold under a vacuum before imaging by a field-emission scanning electron microscope (FESEM, Apreo, Thermo Fisher Scientific, Brno, Czech Republic).

4. Results

4.1. Physical appearance of suspensions and morphologies of ENR nanocomposites

Figures 2a–2d show the physical appearance of the suspensions of ENR/CNT, ENR/CNT-SDS,

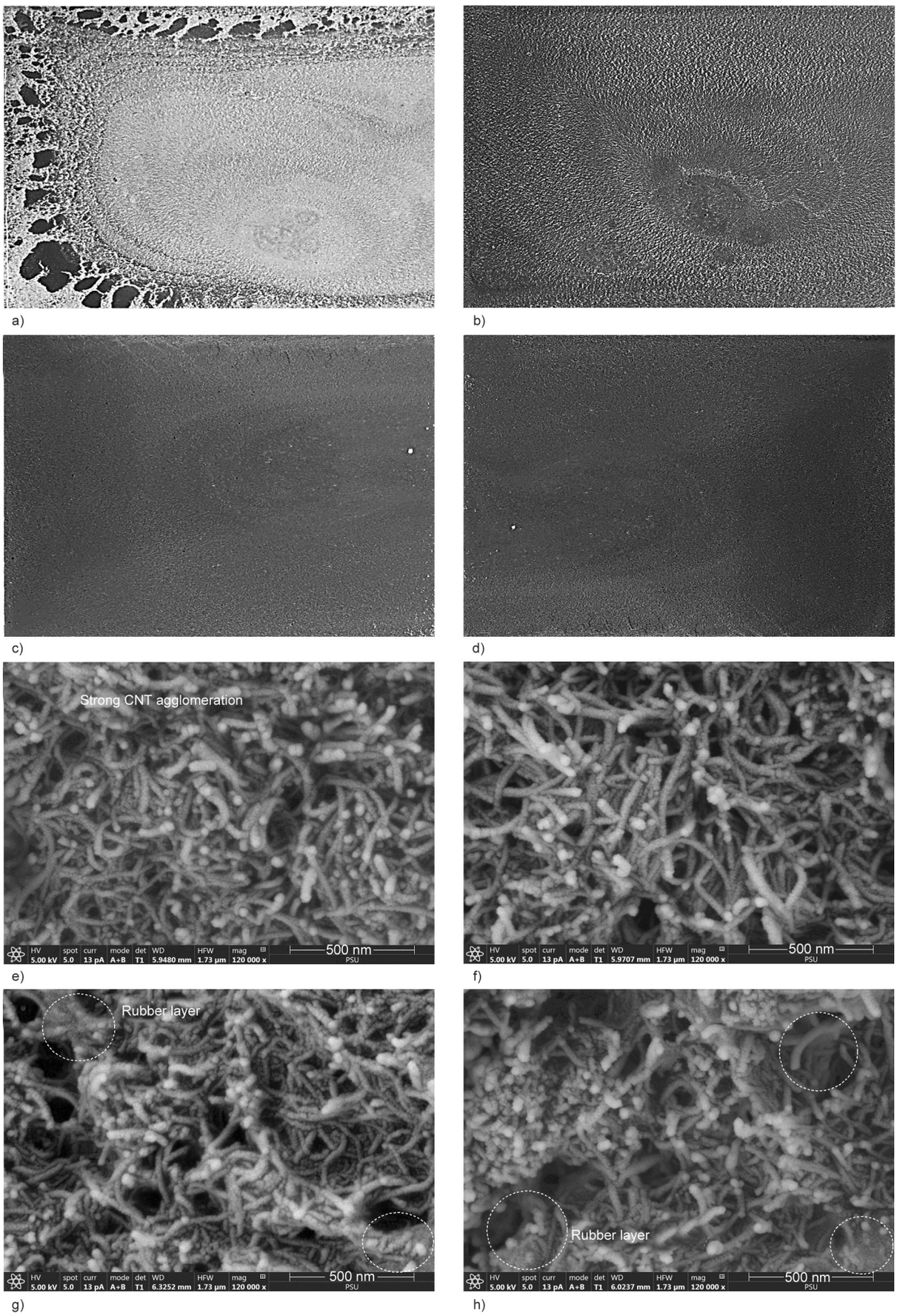

Figure 2. Physical appearance of suspensions, 5 mm wide segments (a, b, c and d) and FESEM micrographs of nanocomposite films (e, f, g and h) for ENR/CNT, ENR/CNT-SDS, ENR/CNT-$Alg_{0.5}$ and ENR/CNT-Alg_1.

ENR/CNT-$Alg_{0.5}$, and ENR/CNT-Alg_1, respectively, and Figures 2e–2h display the morphologies of the nanocomposite films. The homogenization of pre-vulcanized CNT-filled ENR latex can be cursorily estimated by means of the physical appearance of ENR/CNT suspension on the glass plate before drying. Figure 2a displays the ENR/CNT suspension without the surfactant. The unhomogenized ENR/CNT suspension showed the evident separation of pre-vulcanized ENR latex and CNT particles. However, using 0.5% SDS in ENR/CNT nanocomposites provided a better CNT dispersion in the pre-vulcanized ENR latex (Figure 2b). This finding confirmed the role of SDS as a surfactant in the ENR/CNT suspension, as indicated by the proposed model in Figure 3. The mechanism of SDS as a surfactant was the coverage of CNT by SDS molecules in the water media. The hydrophobic tail of SDS interacted with the carbon atoms on the graphite surface of CNTs [23, 24]. Subsequently, the polar head of SDS interacted with water, thus enhancing the dispersion capability of CNTs in aqueous media. Moreover, the remarkable effect of Alg as a surfactant in the ENR nanocomposites was observed (Figure 2c). The loading of 0.5% Alg promoted the homogenized ENR/CNT suspension compared with ENR/CNT-SDS, which indicated that Alg provided prospects as a surfactant for preparing ENR/CNT nanocomposites. The proposed model in Figure 4 can explain this finding. The numerous hydroxyl groups of Alg promoted hydrogen bonding between Alg and the functional groups on the CNT surface. Furthermore, the neutral salt part on sodium Alg structure, in which the carboxyl groups of Alg bonded sodium ions [14], interacted with water, thus enhancing the stability of CNT in water media. Therefore, the increase in Alg in ENR/CNT-Alg resulted in a homogenized suspension (Figure 2d).

The dispersion state of CNT particles in the ENR matrix of ENR/CNT, ENR/CNT-SDS, ENR/CNT-$Alg_{0.5}$, and ENR/CNT-Alg_1 nanocomposite films was estimated from the cross-section of those films. Figures 2e–2h show the FESEM micrographs of the ENR nanocomposites. The intense CNT bundle in Figure 2e indicated the strong CNT agglomeration in the ENR matrix of the ENR/CNT sample. This result was due to the poor dispersion of CNTs in the ENR suspension (Figure 2a). This phenomenon also possibly caused the lowering of the electrical conductivity of ENR/CNT because the dispersion state plays an important role in electrical properties. The introduction of SDS to the ENR nanocomposite provided a looser CNT bundle (Figure 2f). Furthermore, the rubber layer on the filler surface can be noticed in the morphologies of the ENR nanocomposites incorporated with Alg (Figures 2g and 2h). This result indicated the good dispersion of CNT, which promoted stronger rubber–filler interactions [25]. This finding is also directly related to the physical appearance of ENR nanocomposite suspensions

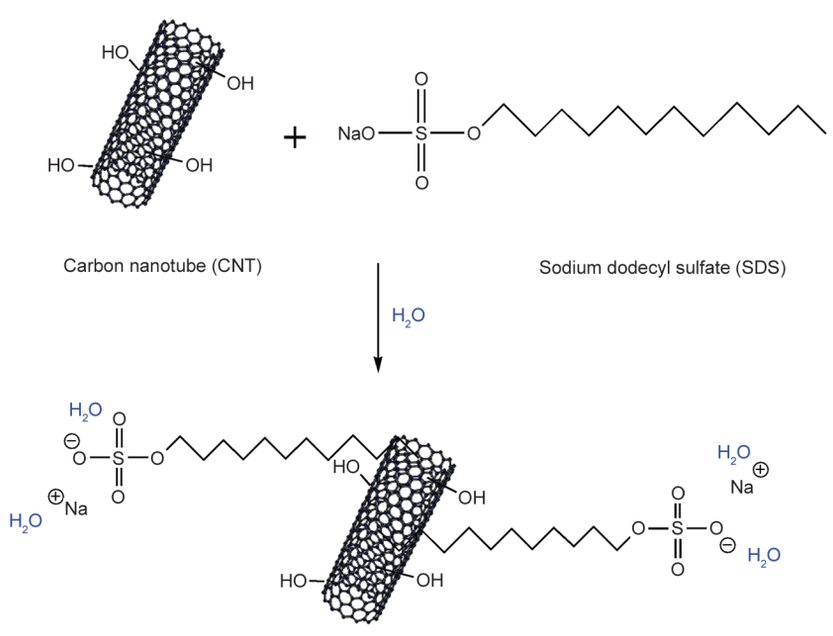

Figure 3. Proposed model of the role of SDS as a surfactant for CNT dispersion in aqueous media.

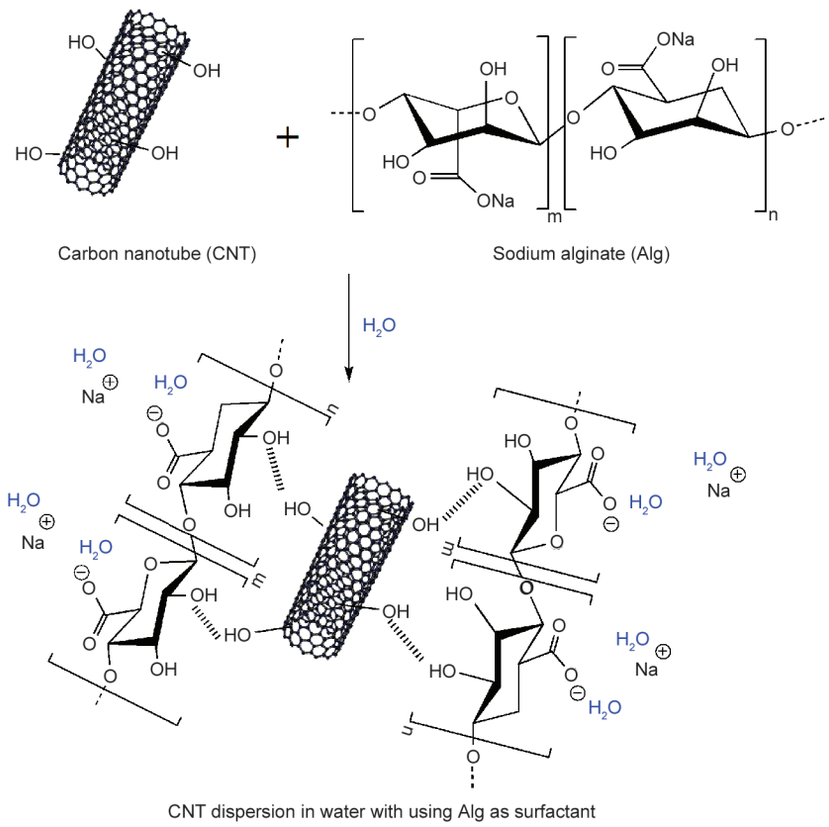

Figure 4. Proposed model of the role of Alg as a surfactant for CNT dispersion in aqueous media.

in Figures 2a–2d; that is, ENR/CNT-Alg$_{0.5}$ and ENR/CNT-Alg$_1$ provided more homogenized suspensions compared with ENR/CNT and ENR/CNT-SDS. Therefore, the role of Alg as a surfactant can be clearly confirmed in terms of the CNT dispersion state via the physical appearance of suspensions and morphological property obtained from FESEM micrographs.

4.2. ATR-FTIR

Figure 5a shows the ATR-FTIR spectra of SDS and Alg powder as surfactants. The spectrum of SDS revealed a broad peak at 3468 cm^{-1}, which corresponded to H–OH stretching. Furthermore, the peaks at the wavenumber of 2955 and 2916 cm^{-1} are assigned to CH_3 and CH_2 asymmetric stretching vibration, respectively, while the peaks at 2852 and 1461 cm^{-1} are assigned to CH_2 symmetric stretching and bending vibration, respectively [26]. Those peaks were associated with long-chain carbon on SDS molecules [26]. The sharp peak at 1216 cm^{-1} was assigned to the skeletal vibration involving the bridge S–O stretch from the polar head part of SDS (Figure 3). The peaks at 1080 and 827 cm^{-1} corresponded to the C–C band stretching and asymmetric C–H bending of the CH_2 group, respectively [27]. The ATR-FTIR spectrum of Alg exhibited a broad peak absorption at 3310 cm^{-1}, which was assigned to the hydroxyl group (–OH) [28, 29] on the Alg structure (Figure 4). Moreover, the peaks at the wavenumber of 1595 and 1406 cm^{-1} referred to the asymmetric and symmetric stretching vibrations of free carboxyl groups, respectively. The peak observed at 1030 cm^{-1} was attributed to the stretching of C–O–C from the –COO groups [30].

Figure 5b exhibits the ATR-FTIR spectra of ENR/CNT nanocomposite films with various surfactants. The characteristic peaks of the ENR matrix were observed at wavenumbers of 2844, 2916, and 2958 cm^{-1}, which indicated C–H stretching. C–H scissoring vibrations were assigned to the absorption peak at 1454 cm^{-1}. The peak at 1375 cm^{-1} also indicated –CH_3 bending vibrations. In ENR, the absorption peaks at 837 and 1595 cm^{-1} corresponded to =C–H wagging and C=C bending vibrations, respectively. Moreover, the epoxirane rings of ENR, which are C–O–C stretching vibrations, were observed at 1103 cm^{-1} [31]. However, the absorption peak at 1343 and 1103 cm^{-1}, which corresponded to the O–H and C–O–C from the epoxirane rings of the

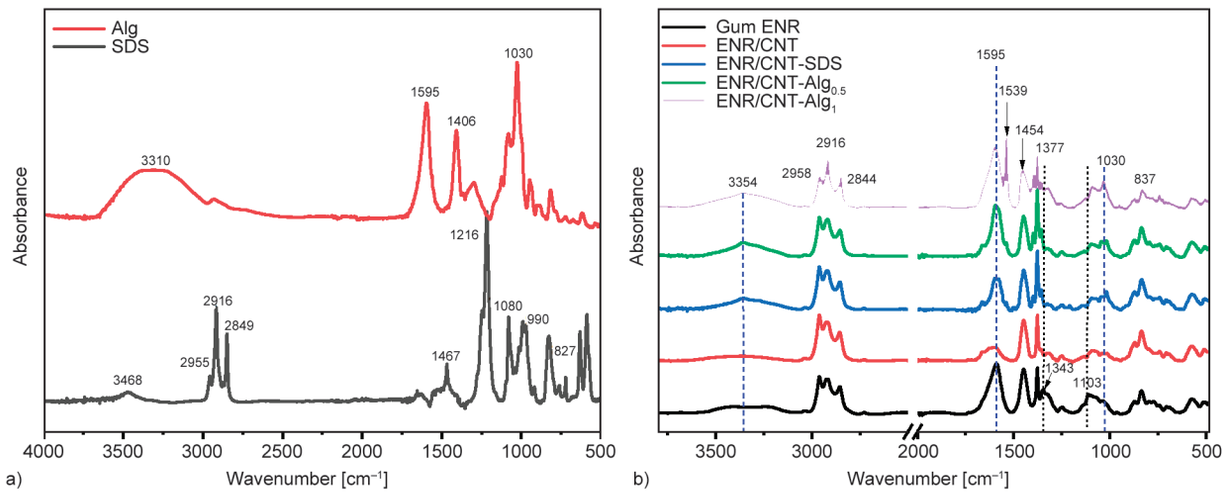

Figure 5. ATR-FTIR spectra of surfactants as sodium alginate (Alg) and sodium dodecyl sulphate (SDS) (a) and its nanocomposite films (b) (gum ENR, ENR/CNT, ENR/CNT-SDS, ENR/CNT-$Alg_{0.5}$ and ENR/CNT-Alg_1 nanocomposite films).

ENR matrix, respectively, significantly decreased with the CNT loading for all samples. This discovery may be attributed to chemical interactions between polar functional groups located in ENR and on CNT surfaces [31]. The addition of CNT reduced C=C bending, as evidenced by a lower peak at 1595 cm^{-1} in ENR/CNT and ENR/CNT-SDS. This was attributed to the interaction of CNTs with double bonds in the rubber molecule [32]. However, due to the peak overlap of the double bond in ENR and the free carboxyl groups in Alg. As a result, increasing Alg gave a higher peak intensity of 1595 cm^{-1}. Moreover, the height of the peak increased with the loading of Alg, as proven by the highest peak of ENR/CNT-Alg_1. In addition, the existence of surfactants in the ENR nanocomposite films led to the increased peak at the wavenumber of 3354 cm^{-1}, which corresponded to the OH group in the SDS and Alg structures, for ENR/CNT-SDS, ENR/CNT-$Alg_{0.5}$, and ENR/CNT-Alg_1. Furthermore, the increased loading of Alg in the ENR/CNT-Alg_1 film resulted in the peak of C–O–C stretching at the wavenumber of 1030 cm^{-1}, which led to the increased incorporation of the Alg structure in the ENR nanocomposites.

4.3. Mechanical properties and crosslinking of ENR nanocomposite films

The mechanical properties of ENR/CNT nanocomposite films were indicated in terms of thestress–strain curve in Figure 6a, and the details are shown in Table 2. The increases in the 100 and 300% moduli with the addition of CNT were observed, and they were caused by the presence of a non-stretchable rigid filler (CNT), which led to the strain amplification effect. On the other hand, the addition of 5 phr CNT to the ENR matrix in the absence of any surfactant caused the lowering of tensile strength and elongation at break. This finding was due to the rigidity of CNT agglomeration (Figure 2e) in the ENR matrix, which can act as a weak point in the ENR nanocomposite. This poor filler dispersion in the matrix for ENR/CNT nanocomposite without surfactant correlated well with the physical appearance shown in Figure 2a. In addition, the decreased tensile strength and elongation at break were also noted in the ENR/CNT-SDS nanocomposites. In fact, the interaction between ENR and SDS contributed to the colloidal stability of ENR latex. This is due to the hydrophilic head of SDS being oriented toward the

Table 2. 100, 300% modulus, tensile strength, and elongation at break of gum ENR, ENR/CNT, ENR/CNT-SDS, ENR/CNT-$Alg_{0.5}$ and ENR/CNT-Alg_1 nanocomposite films.

Samples	100% Modulus [MPa]	300% Modulus [MPa]	Tensile strength [MPa]	Elongation at break [%]
Gum ENR	0.73±0.04	2.33±0.06	11.82±0.58	521.88±12.17
ENR/CNT	1.09±0.08	3.10±0.18	5.96±1.33	326.95±5.07
ENR/CNT-SDS	1.49±0.24	3.86±0.23	4.30±0.96	382.89±3.81
ENR/CNT-$Alg_{0.5}$	1.52±0.62	4.15±0.17	6.43±0.61	384.06±26.94
ENR/CNT-Alg_1	1.59±0.05	4.52±0.07	12.24±0.64	468.10±9.02

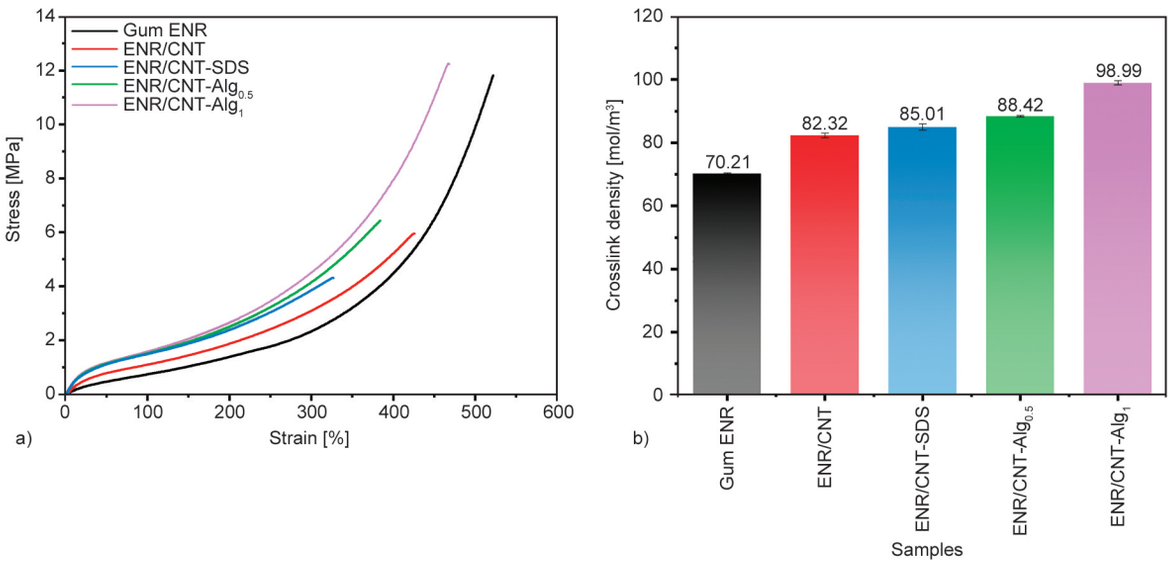

Figure 6 Stress-strain curve (a) and crosslink density (b) of gum ENR, ENR/CNT, ENR/CNT-SDS, ENR/CNT-$Alg_{0.5}$, and ENR/CNT-Alg_1 nanocomposite films.

aqueous medium in the latex system, resulting in an increase in the electrical charge of the latex particles' surfaces and then providing greater system stability [33]. On the other hand, the decrease in tensile strength and elongation at break can be attributed to the coalescence of SDS, which acted as defects in the nanocomposite film and the ENR matrix [12, 34]. Nevertheless, the ENR/CNT-SDS provided 100 and 300% higher moduli than gum ENR and ENR/CNT, which indicated the more homogeneous dispersion of CNTs in the ENR matrix. The enhancement of tensile properties was obtained when using Alg as the surfactant for ENR nanocomposites. At the equivalent surfactant loading (0.5% ENR latex), the ENR/CNT-$Alg_{0.5}$ nanocomposite gave 100 and 300% higher moduli, tensile strength, and elongation at break than the ENR/CNT-SDS. This finding was attributed to the improved CNT dispersion in the ENR matrix of ENR/CNT-$Alg_{0.5}$ nanocomposites. This result also corresponded well to the physical appearance of ENR nanocomposite suspension in Figure 2. The ENR/CNT-$Alg_{0.5}$ nanocomposite (Figure 2c) exhibited a more homogenized suspension than ENR/CNT-SDS nanocomposites (Figure 2b). Moreover, the increase in Alg to 1% improved mechanical properties, as exhibited by the dramatic increase in the tensile strength and elongation at break. This result implied that the use of Alg successfully promoted the fine dispersion of CNTs, which supported more filler–rubber interaction in the ENR nanocomposite film.

Furthermore, the crosslink density of the gum ENR and ENR nanocomposites were evaluated by a swelling method using the Flory–Rehner equation. As shown in Figure 6b, the incorporation of CNTs in the NR matrix resulted in increased crosslink density. This result was due to the physical crosslink between CNTs and the ENR matrix, which immobilized the rubber chains [35], thus preventing them from swelling. Furthermore, applying a surfactant in the ENR nanocomposites enhanced the crosslink density. The crosslink density slightly increased in ENR/CNT-SDS nanocomposites compared with those in ENR/CNT. This finding can be attributed to the better CNT network formed in the ENR matrix with the improvement of filler dispersion through the addition of SDS, which resulted in the increased generation of the physical crosslink among CNTs and the ENR matrix. In addition, a higher crosslink density was observed in ENR/CNT-$Alg_{0.5}$ compared with ENR/CNT-SDS, which indicated better CNT dispersion in the ENR in the presence of 0.5% Alg. This result correlated well with the physical appearance of ENR nanocomposite suspension in Figure 2, which shows that a more homogenized suspension was noted in ENR/CNT-$Alg_{0.5}$ compared with ENR/CNT-SDS. Furthermore, the increase in Alg to 1% in ENR/CNT-Alg_1 provided the highest crosslink density compared with those of ENR/CNT, ENR/CNT-SDS, and ENR/CNT-$Alg_{0.5}$. As mentioned previously, the improved network formation of CNT, which was affected by fine filler dispersion, promoted the increase in the crosslink density. Therefore, the effectiveness of Alg in improving filler dispersion in the ENR matrix can be confirmed.

4.4. Hysteresis loss

Figure 7 presents the hysteresis loss of ENR/CNT nanocomposite films with various surfactants. This result was used to calculate the Mullins effect, which indicated the change in the structure of the connections of fillers in the rubber matrix while cyclic loading [36]. The stress–strain loops at 50, 100, and 300% strains (Figures 7a–7c, respectively) represented the hysteresis loss at different strain conditions [37]. Thus, all samples' hysteresis loss with various strains (Figure 7d) was integrated from the stress–strain loop areas. Gum ENR provided the lowest hysteresis loss at all cyclic strain levels due to the elastic-like behavior of rubber. However, the ENR nanocomposites filled with CNTs exhibited a higher hysteresis loss than the gum ENR. This finding was due to the Mullins effect, which affected the breakdown of the CNT network under cyclic strain application. In addition, the hysteresis loss of ENR/CNT, ENR/CNT-SDS, ENR/CNT-$Alg_{0.5}$, and ENR/CNT-Alg_1 nanocomposites increased with the increase in cyclic strain loading. This finding confirmed that the filler network in the ENR matrix became more damaged with the increase in applied cyclic strain. In addition, the effect of the incorporation of surfactants in the nanocomposites revealed a higher hysteresis loss than the ENR/CNT without surfactant. This result confirmed that ENR/CNT-SDS, ENR/CNT-$Alg_{0.5}$, and ENR/CNT-Alg_1 generated a better network than ENR/CNT. As shown by the proposed model in Figure 8a, the surfactants promoted the network formation of CNT, which can be damaged under strain loading, resulting in hysteresis loss. Although the poor dispersion of CNTs in ENR/CNT might have caused the single-CNT agglomeration in the ENR matrix from the breaking down of intense CNT agglomeration with strain loading (Figure 8b), this condition had a lower effect on hysteresis loss than the damage of the CNT network. However, various types of surfactants (*i.e.*, SDS and Alg) exhibited slight differences in hysteresis loss. Nevertheless, differences were observed when the high cyclic strain of 300%

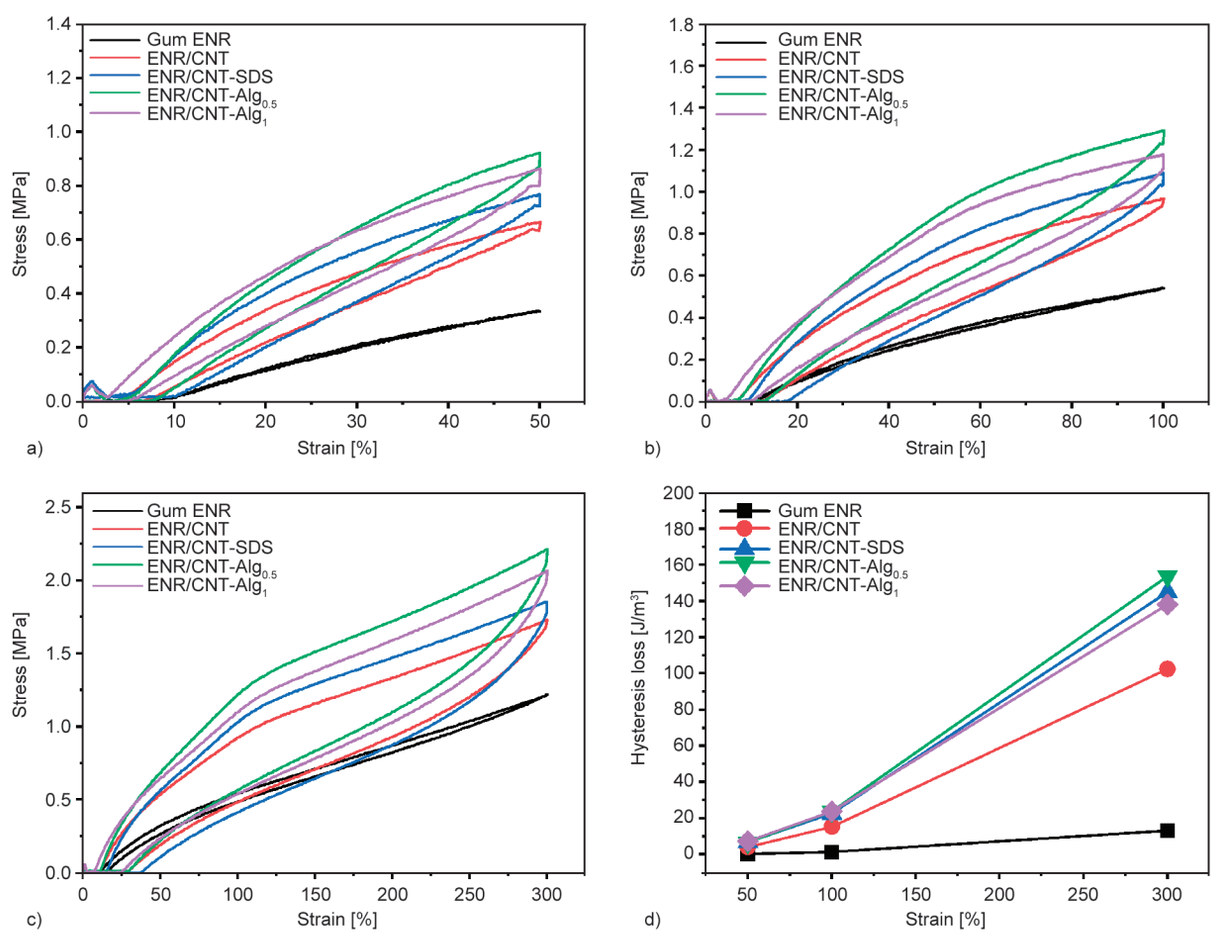

Figure 7. Hysteresis loss of gum ENR, ENR/CNT, ENR/CNT-SDS, ENR/CNT-$Alg_{0.5}$ and ENR/CNT-Alg_1 nanocomposite films: a) stress–strain loops at 50%, b) 100%, c) 300% and d) hysteresis loss at various strain.

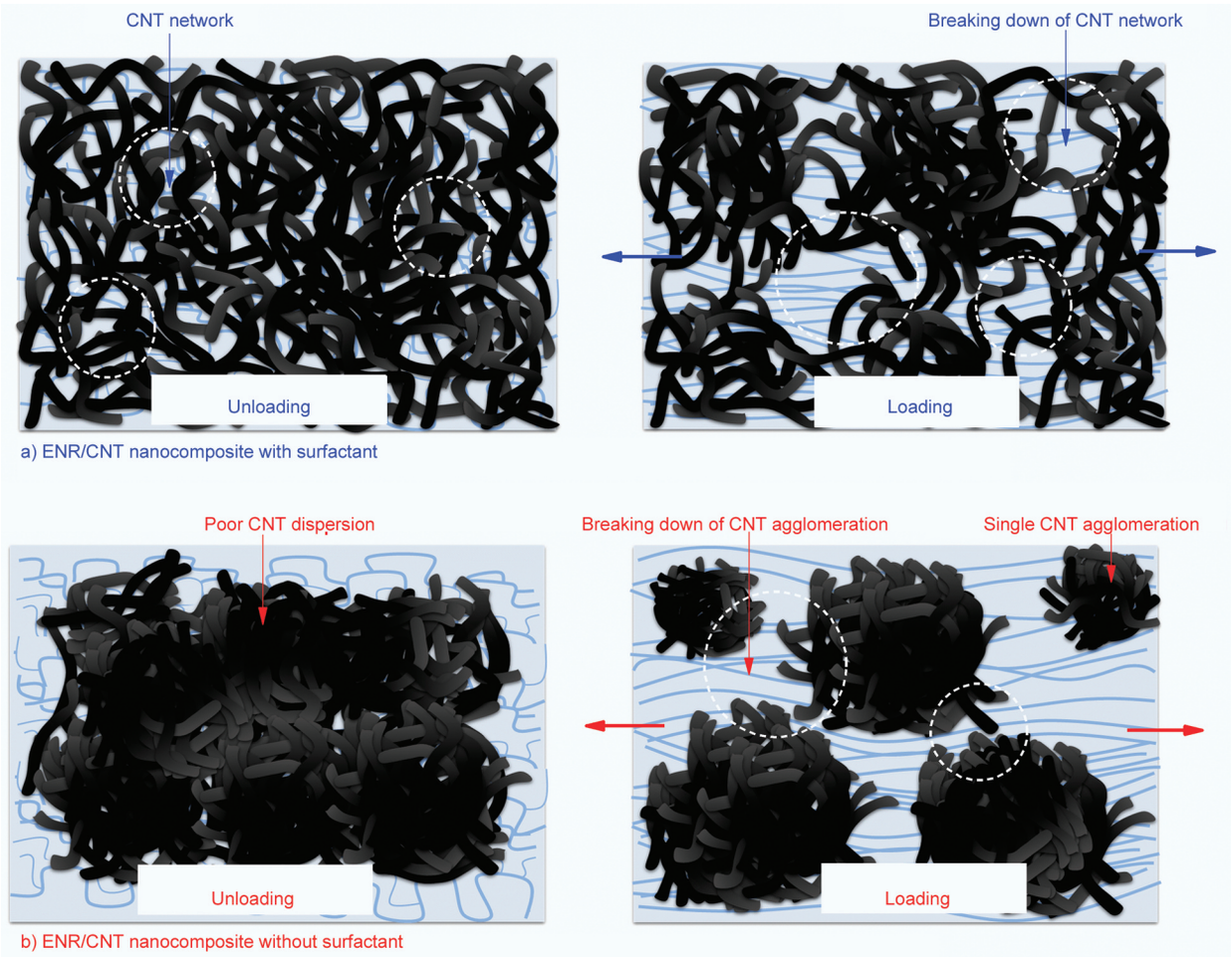

Figure 8. Proposed model of ENR/CNT nanocomposites with (a) and without (b) surfactants under unloading and loading.

was applied. The ENR/CNT-Alg$_{0.5}$ showed the highest hysteresis loss, followed by ENR/CNT-SDS, and ENR/CNT-Alg$_1$ exhibited the lowest. The low hysteresis loss at a high cyclic strain loading can be attributed to the filler network, which cannot be damaged [38]. Thus, ENR/CNT-Alg$_1$ generated a stronger network than ENR/CNT-Alg$_{0.5}$ and ENR/CNT-SDS. This result may be due to the higher surfactant loading in ENR/CNT-Alg$_1$, which supported the stronger CNT network in the ENR matrix.

4.5. Dynamic mechanical property

The dynamic mechanical property of ENR/CNT nanocomposites was estimated by means of storage modulus and Tanδ as functions of temperature (Figures 9, respectively). The details are shown in Table 3. Three zones were evidently observed from the storage modulus curve in Figure 9a: glassy, glass transition, and rubbery flow regions. In the glassy state, the mobility of rubber molecules is restricted [25]. On the other hand, in the rubbery state, the mobility of rubber molecules is unrestricted. The introduction of CNTs to the ENR matrix tremendously increased the storage modulus in glassy and rubbery flow states, as noted in the storage modulus observed at –40 and 25 °C (Table 3). This finding confirmed the effective reinforcement of CNT particles in the ENR matrix in a wide temperature range. The variable surfactants in the ENR nanocomposites showed slight differences in storage moduli in the glassy state. However, in the rubbery flow region, the ENR/CNT-Alg$_1$ exhibited the highest storage modulus. The storage modulus at 25 °C was 24.64 MPa, and those for ENR/CNT, ENR/CNT-SDS, and ENR/CNT-Alg$_{0.5}$ were 10.25, 8.40, and 8.45 MPa, respectively. This finding correlated well to the 100 and 300% moduli in Figures 6a and Table 2 and was due to the higher homogeneous dispersion of CNT in the ENR/CNT-Alg$_1$ nanocomposite, which promoted the filler–rubber interaction. In addition, the glass transition temperature (T_g) of ENR nanocomposites was noted from the tanδ peak in Figure 9b and the data in Table 3. Gum ENR provided the T_g at –34.50 °C. The addition of CNT shifted the T_g of ENR/CNT

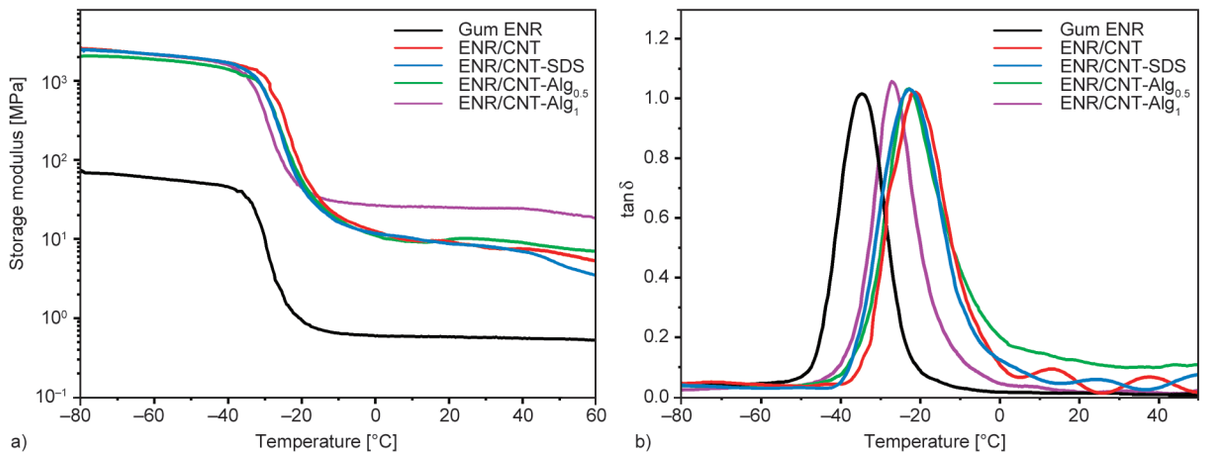

Figure 9. Storage modulus (a) and tan δ (b) as functions of temperature for gum ENR, ENR/CNT, ENR/CNT-SDS, ENR/CNT-$Alg_{0.5}$, and ENR/CNT-Alg_1 nanocomposite films.

Table 3. Glass transition temperature (T_g), storage modulus at –40 and 25 °C of gum ENR, ENR/CNT, ENR/CNT-SDS, ENR/CNT-$Alg_{0.5}$ and ENR/CNT-Alg_1 nanocomposite films.

Samples	T_g [°C]	Storage modulus at –40 °C [MPa]	Storage modulus at 25 °C [MPa]
Gum ENR	–34.50	46.16	0.56
ENR/CNT	–21.22	1712.40	8.45
ENR/CNT-SDS	–22.40	1717.86	8.40
ENR/CNT-$Alg_{0.5}$	–22.71	1412.66	10.25
ENR/CNT-Alg_1	–26.91	1625.17	24.62

nanocomposites to –21.22 °C because CNT agglomeration in the ENR matrix may restrict the mobility of NR chains. However, the introduction of SDS and Alg to ENR nanocomposites affected the reduction of T_g to –22.40, –22.71, and –26.91 °C for ENR/CNT-SDS, ENR/CNT-$Alg_{0.5}$, and ENR/CNT-Alg_1, respectively. This finding was due to the surfactant-favored movement of ENR chains, resulting in better ENR chain mobility compared with the ENR nanocomposites without a surfactant.

4.6. Electrical properties

Figure 10a exhibits electrical conductivity as a function of the frequency of gum ENR and ENR/CNT nanocomposite films with various surfactants calculated from Equation (2). The electrical conductivity depending on frequency, can be noted for all samples. This dependence resulted from an approximation of an exponential power law, indicating a conductivity hopping mechanism [39]. Hopping was simulated at a high frequency, which resulted in increased conductivity. Incorporating CNT into the ENR nanocomposites dramatically increased the electrical conductivity of ENR/CNT nanocomposites. This finding indicated the enhancement of extreme conductive properties of CNT with its sp^2 hybridized

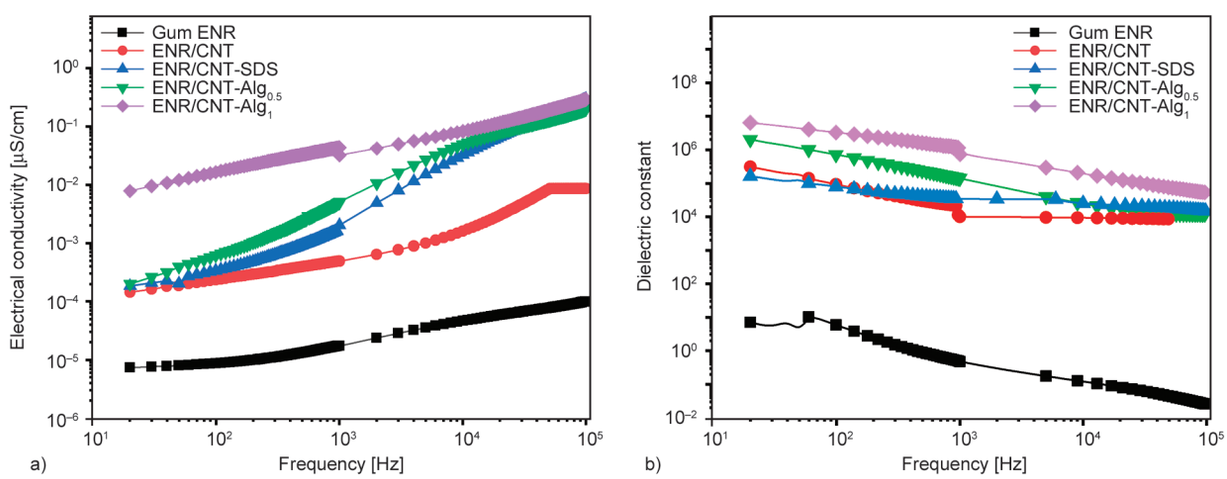

Figure 10. Electrical conductivity (a) and dielectric constant (b) of gum ENR, ENR/CNT, ENR/CNT-SDS, ENR/CNT-$Alg_{0.5}$, and ENR/CNT-Alg_1 nanocomposite films.

structures. Consequently, the conductive network of CNTs in ENR matrix enhanced the conductive property of NR composites [40]. Therefore, the dispersion state of CNTs in the rubber matrix was the main parameter at electrical conductivity levels. As observed under the same loading of CNTs, the ENR/CNT, ENR/CNT-SDS, ENR/CNT-$Alg_{0.5}$, and ENR/CNT-Alg_1 nanocomposites provided tremendous differences in terms of electrical conductivity. The ENR/CNT nanocomposite film gave the lowest electrical conductivity due to the poor dispersion of CNT, which lowered the formation of the CNT network in the ENR matrix. This finding corresponded well with the physical appearance of the ENR/CNT suspension in Figure 2a, which shows that an unhomogenized suspension was generated. However, the electrical conductivity improved in the presence of surfactants (*i.e.*, SDS and Alg) due to the excellent dispersion state of CNTs in such conditions. Furthermore, at the 0.5% surfactant loading, the results revealed that ENR/CNT-$Alg_{0.5}$ gave a higher electrical conductivity than ENR/CNT-SDS. This finding corresponded to the dispersion of CNTs in aqueous media, as shown in Figures 2b and 2c; that is, ENR/CNT-$Alg_{0.5}$ showed a more homogenized suspension than ENR/CNT-SDS. Hence, sodium Alg can be a potential surfactant that enhances the conductive property of ENR nanocomposite films prepared by the latex technique. In addition, 1% Alg loading in ENR/CNT-Alg_1 exhibited a considerable increase in electrical conductivity.

Figure 10b shows the dielectric constant of gum ENR and ENR/CNT nanocomposite films. The addition of CNTs to the ENR matrix provided a huge effect on the increase in the dielectric constant. It was attributed to the sp^2-hybridization of CNTs, which resulted in a large number of free electrons forming electric dipoles. Hence, the dipole-dipole interaction of the rubber and filler particles caused the CNT particles in the rubber matrix to act as a dipole, resulting in the occurrence of interfacial polarization. [41]. Furthermore, the use of SDS in ENR/CNT-SDS showed less effect on the dielectric constant of ENR nanocomposites. However, the incorporation of Alg enhanced the dielectric constant. The dielectric constant of ENR/CNT-$Alg_{0.5}$ was higher observed compared with those of ENR/CNT and ENR/CNT-SDS. Moreover, the higher Alg loading in ENR/CNT-Alg_1 supported the increase in the dielectric constant; that is, ENR/CNT-Alg_1 gave the highest dielectric constant. This result was the effect of interfacial polarization, which was generated more in ENR/CNT-Alg_1 nanocomposite owing to the higher polar group of Alg in the ENR nanocomposite. As confirmed by the chemical structure and ATR-FTIR spectrum in Figures 5, Alg had plenty of hydroxyl groups in its structure.

4.7. Piezoresistivity

Figure 11 shows piezoresistivity in relation to the change of resistance per unit change of strain ($\Delta R/R_0$) and time under cyclic stretching. The strain sensitivity of the ENR nanocomposite films was indicated in terms of piezoresistivity. Piezoresistivity is the ability of the conductive material to change resistance with mechanical force [42]. Figure 11a shows that ENR/CNT exhibited variation in changing in resistance ($\Delta R/R_0$) with applied cyclic strain. This discovery was made possible by the permanent damage to CNT conducting pathways caused by several loading cycles [8]. In other words, the damaged CNT had lower conductivity because electrical charges could not move through nanocomposites, causing unstable $\Delta R/R_0$ values of ENR/CNT nanocomposite. However, a low conductive network formed in the ENR/CNT nanocomposite film due to poor CNT dispersion. This result correlated well with the physical appearance shown in Figure 2a, morphology in Figure 2e, and electrical conductivity in Figure 10a. However, the strain sensitivity of ENR nanocomposites improved with the addition of surfactants. As noted in Figure 11b, ENR/CNT-SDS exhibited a more stable $\Delta R/R_0$ and higher sensitivity compared with ENR/CNT, which indicated the arrangement of fillers within the rubber matrix creates a more stable and resilient conducting network [8]. This result was due to the fine dispersion of CNTs in the ENR matrix induced with the exiting of SDS. Moreover, the stable change in resistance under cyclic strain was noted in ENR/CNT-$Alg_{0.5}$ (Figure 11c). This result was attributed to the effectiveness of Alg as a surfactant that supported the dispersion of CNTs in aqueous media, resulting in good dispersion in the ENR matrix and conductive network formation. Accordingly, the stable change in resistance caused by the steady and resilient conducting network of CNTs was also observed under increased loading of Alg in ENR/CNT-Alg_1. However, ENR/CNT-$Alg_{0.5}$ and ENR/CNT-Alg_1 exhibited lower $\Delta R/R_0$ than ENR/CNT-SDS, this explains why the entangled and

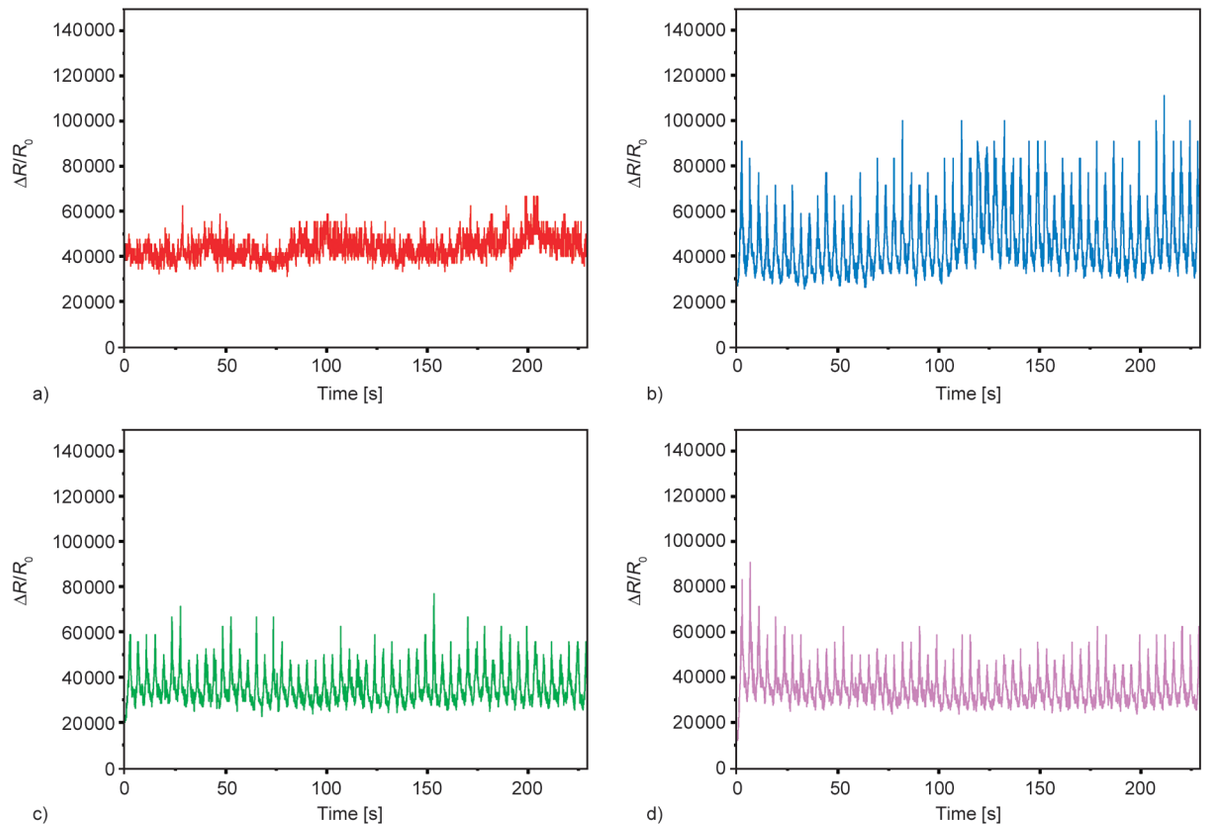

Figure 11. Piezoresistivity of ENR/CNT (a), ENR/CNT-SDS (b), ENR/CNT-$Alg_{0.5}$ (c) and ENR/CNT-Alg_1 (d) nanocomposite films.

flexible nature of conducting connectivity can enhance the decrease in piezoresistivity ($\Delta R/R_0$), *i.e.* the conducting routes are not broken at low or relatively high strain [38]. Therefore, the strong interaction among CNT conductive networks in the ENR nanocomposites was promoted with the use of Alg as a surfactant compared with SDS. This finding corresponded well to the mechanical properties (Figure 6a), hysteresis loss (Figure 7), and electrical conductivity (Figure 10a). In addition, Figure 12 shows the strain-sensing behaviors for finger bending of ENR/CNT nanocomposite films with surfactants. The samples were prepared by gluing two copper tape electrodes on the ends of a composite strip with silver paste [43] (Figure 12a). The copper wires were joined to both sides of the electrodes and connected to the resistance measurement device (Figure 12b). After the strain sensor was attached to the forefinger joint, repeated bending-straightening motions were performed as indicated in Figure 12c. The ENR/CNT-SDS, ENR/CNT-$Alg_{0.5}$, and ENR/CNT-Alg_1 provided no significant difference in the reflection of resistance on finger motion. Thus, the $\Delta R/R_0$ increased during finger joint bending to a certain angle under which the samples were stretching. On the other hand, returning the finger joint to its straightening state decreased $\Delta R/R_0$ due to its return to its original position. This finding demonstrated well that the ENR nanocomposite films can be used in strain sensor applications.

5. Conclusion

This study proposed a novel surfactant for the preparation of ENR/CNT nanocomposite films by a latex processing method. We utilized the fine dispersion of CNTs in the ENR matrix to achieve suitable nanocomposites for strain sensors. The physical appearance of the ENR/CNT suspension revealed that using Alg as a surfactant supported a more homogeneous ENR/CNT suspension than SDS. In addition, the higher percentage of Alg in the ENR nanocomposites as ENR/CNT/Alg_1 promoted a more homogeneous suspension. Therefore, using Alg as a surfactant promoted finer CNT dispersion in ENR nanocomposites and filler–rubber interaction, as confirmed by FESEM images. This condition improved the mechanical and electrical properties and strain sensitivity of ENR/CNT nanocomposites by incorporating Alg. This result

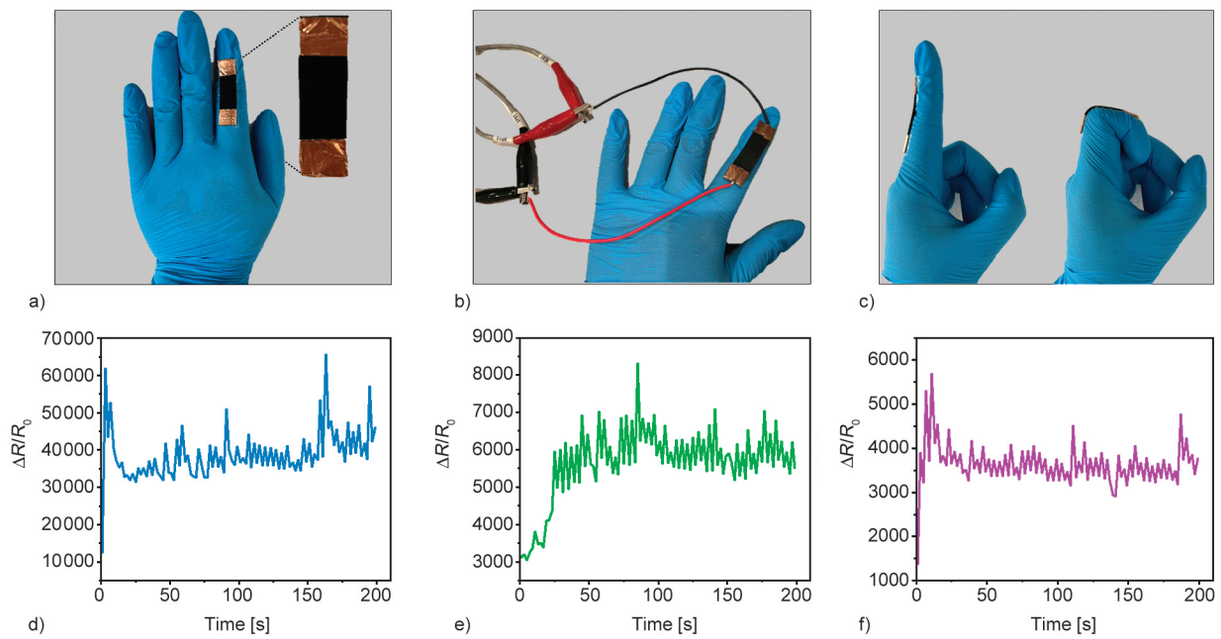

Figure 12. The strain sensing behaviors for finger bending of ENR/CNT-SDS (d), ENR/CNT-$Alg_{0.5}$ (e), and ENR/CNT-Alg_1 (f) nanocomposite films.

implied that Alg could be a high-potential candidate as a surfactant in the preparation of ENR/CNT strain sensor films. In addition, the ENR nanocomposite films from the latex technology mixing can be used in strain sensor applications, as confirmed by their sensitivity in finger motion.

Acknowledgements

This work was supported by Ratchadapisek Somphot Fund for Postdoctoral Fellowship, Chulalongkorn University. GAICCE Research Grant from ASEAN University Network/Southeast Asia Engineering Education Development Network is also acknowledged.

References

[1] Hu N., Karube Y., Arai M., Watanabe T., Yan C., Li Y., Liu Y., Fukunaga H.: Investigation on sensitivity of a polymer/carbon nanotube composite strain sensor. Carbon, **48**, 680–687 (2010). https://doi.org/10.1016/j.carbon.2009.10.012

[2] Kurian A. S., Giffney T., Lee J., Travas-Sejdic J., Aw K. C.: Printing of CNT/silicone rubber for a wearable flexible stretch sensor. in 'Proceedings of Electroactive Polymer Actuators and Devices (EAPAD) 2016. Las Vegas' Vol. 9798, 28–35 (2016). https://doi.org/10.1117/12.2218224

[3] Kang I., Schulz M. J., Kim J. H., Shanov V., Shi D.: A carbon nanotube strain sensor for structural health monitoring. Smart Materials and Structures, **15**, 737 (2006). https://doi.org/10.1088/0964-1726/15/3/009

[4] Zhang W., Suhr J., Koratkar N.: Carbon nanotube/polycarbonate composites as multifunctional strain sensors. Journal of Nanoscience and Nanotechnology, **6**, 960–964 (2006). https://doi.org/10.1166/jnn.2006.171

[5] Loh K. J., Lynch J. P., Shim B., Kotov N.: Tailoring piezoresistive sensitivity of multilayer carbon nanotube composite strain sensors. Journal of Intelligent Material Systems and Structures, **19**, 747–764 (2008). https://doi.org/10.1177/1045389X07079872

[6] Chang F-Y., Wang R-H., Yang H., Lin Y-H., Chen T-M., Huang S-J.: Flexible strain sensors fabricated with carbon nano-tube and carbon nano-fiber composite thin films. Thin Solid Films, **518**, 7343–7347 (2010). https://doi.org/10.1016/j.tsf.2010.04.108

[7] Nakaramontri Y., Kummerlöwe C., Nakason C., Pichaiyut S., Wisunthon S., Clemens F.: Piezoresistive carbon-based composites for sensor applications: Effects of polarity and non-rubber components on shape recovery. Express Polymer Letters, **14**, 970–986 (2020). https://doi.org/10.3144/expresspolymlett.2020.79

[8] Natarajan T. S., Eshwaran S. B., Stöckelhuber K. W., Wießner S., Pötschke P., Heinrich G., Das A.: Strong strain sensing performance of natural rubber nanocomposites. ACS Applied Materials and Interfaces, **9**, 4860–4872 (2017). https://doi.org/10.1021/acsami.6b13074

[9] Grossiord N., Hermant M. C.: Latex technology for conductive polymer nanocomposites. in 'Encyclopedia of Polymer Science and Technology' (ed.: Mark H. F.) Wiley, New York, 1–25 (2002). https://doi.org/10.1002/0471440264.pst506.pub2

[10] Nakaramontri Y., Nakason C., Kummerlöwe C., Vennemann N.: Enhancement of electrical conductivity and filler dispersion of carbon nanotube filled natural rubber composites by latex mixing and *in situ* silanization. Rubber Chemistry and Technology, **89**, 272–291 (2016). https://doi.org/10.5254/rct.15.84848

[11] Bhattacharyya S., Sinturel C., Bahloul O., Saboungi M-L., Thomas S., Salvetat J-P.: Improving reinforcement of natural rubber by networking of activated carbon nanotubes. Carbon, **46**, 1037–1045 (2008). https://doi.org/10.1016/j.carbon.2008.03.011

[12] Aguilar-Bolados H., Yazdani-Pedram M., Brasero J., Lopez-Manchado M. A.: Influence of the surfactant nature on the occurrence of self-assembly between rubber particles and thermally reduced graphite oxide during the preparation of natural rubber nanocomposites. Journal of Nanomaterials, **2015**, 212493 (2015). https://doi.org/10.1155/2015/212493

[13] Supanakorn G., Varatkowpairote N., Taokaew S., Phisalaphong M.: Alginate as dispersing agent for compounding natural rubber with high loading microfibrillated cellulose. Polymers, **13**, 468 (2021). https://doi.org/10.3390/polym13030468

[14] dos Santos L. A. L.: Natural polymeric biomaterials: Processing and properties. Materials Science and Materials Engineering, **2017**, 1–6 (2017). https://doi.org/10.1016/B978-0-12-803581-8.02253-0

[15] Zaman H. U., Beg M. D. H.: Preparation and properties of sodium alginate films. Journal of Polymer Engineering, **33**, 829–836 (2013). https://doi.org/10.1515/polyeng-2013-0146

[16] Theagarajan R., Dutta S., Moses J. A., Anandharamakrishnan C.: Alginates for food packaging applications. Alginates for food polysaccharides and their applications' (ed.: Shakeel A.) Taylor and Francis, Florida, 207–232 (1995). https://doi.org/10.1002/9781119487999.ch11

[17] Kwok K. K., Groves M. J., Burgess D. J.: Production of 5–15 μm diameter alginate-polylysine microcapsules by an air-atomization technique. Pharmaceutical Research, **8**, 341–344 (1991). https://doi.org/10.1023/A:1015841531372

[18] Flory P. J., Rehner J.: Statistical mechanics of cross-linked polymer networks I. Rubberlike elasticity. The Journal of Chemical Physics, **11**, 512–520 (1943). https://doi.org/10.1063/1.1723791

[19] Flory P. J.: Molecular size distribution in three dimensional polymers. II. Trifunctional branching units. Journal of the American Chemical Society, **63**, 3091–3096 (1941). https://doi.org/10.1021/ja01856a062

[20] Gelling I., Tinker A., bin Abdul Rahman H.: Solubility parameters of epoxidised natural rubber. Journal of Natural Rubber Research (Malaysia), **20**, 20–29 (1991).

[21] Du F., Fischer J. E., Winey K. I.: Coagulation method for preparing single-walled carbon nanotube/poly(methyl methacrylate) composites and their modulus, electrical conductivity, and thermal stability. Journal of Polymer Science Part B: Polymer Physics, **41**, 3333–3338 (2003). https://doi.org/10.1002/polb.10701

[22] Safadi B., Andrews R., Grulke E.: Multiwalled carbon nanotube polymer composites: Synthesis and characterization of thin films. Journal of Applied Polymer Science, **84**, 2660–2669 (2002). https://doi.org/10.1002/app.10436

[23] Domínguez H.: Self-aggregation of the SDS surfactant at a solid−liquid interface. The Journal of Physical Chemistry B, **111**, 4054–4059 (2007). https://doi.org/10.1021/jp067768b

[24] Tummala N. R., Striolo A.: SDS surfactants on carbon nanotubes: Aggregate morphology. ACS Nano, **3**, 595–602 (2009). https://doi.org/10.1021/nn8007756

[25] Krainoi A., Kummerlöwe C., Nakaramontri Y., Wisunthorn S., Vennemann N., Pichaiyut S., Kiatkamjornwong S., Nakason C.: Novel natural rubber composites based on silver nanoparticles and carbon nanotubes hybrid filler. Polymer Composites, **41**, 443–458 (2020). https://doi.org/10.1002/pc.25378

[26] Gao X., Chorover J.: Adsorption of sodium dodecyl sulfate (SDS) at ZnSe and α-Fe_2O_3 surfaces: Combining infrared spectroscopy and batch uptake studies. Journal of Colloid and Interface Science, **348**, 167–176 (2010). https://doi.org/10.1016/j.jcis.2010.04.011

[27] Singh M. K., Agarwal A., Gopal R., Swarnkar R. K., Kotnala R. K.: Dumbbell shaped nickel nanocrystals synthesized by a laser induced fragmentation method. Journal of Materials Chemistry, **21**, 11074–11079 (2011). https://doi.org/10.1039/c1jm12320c

[28] Han J., Zhou Z., Yin R., Yang D., Nie J.: Alginate–chitosan/hydroxyapatite polyelectrolyte complex porous scaffolds: Preparation and characterization. International Journal of Biological Macromolecules, **46**, 199–205 (2010). https://doi.org/10.1016/j.ijbiomac.2009.11.004

[29] Pongjanyakul T.: Alginate–magnesium aluminum silicate films: Importance of alginate block structures. International Journal of Pharmaceutics, **365**, 100–108 (2009). https://doi.org/10.1016/j.ijpharm.2008.08.025

[30] Adzmi F., Meon S., Musa M. H., Yusuf N. A.: Preparation, characterisation and viability of encapsulated *Trichoderma harzianum* UPM40 in alginate-montmorillonite clay. Journal of Microencapsulation, **29**, 205–210 (2012). https://doi.org/10.3109/02652048.2012.659286

[31] Krainoi A., Kummerlöwe C., Nakaramontri Y., Vennemann N., Pichaiyut S., Wisunthorn S., Nakason C.: Influence of critical carbon nanotube loading on mechanical and electrical properties of epoxidized natural rubber nanocomposites. Polymer Testing, **66**, 122–136 (2018). https://doi.org/10.1016/j.polymertesting.2018.01.003

[32] Krainoi A., Kummerlöwe C., Nakaramontri Y., Wisunthorn S., Vennemann N., Pichaiyut S., Kiatkamjornwong S., Nakason C.: Influence of carbon nanotube and ionic liquid on properties of natural rubber nanocomposites. Express Polymer Letters, **13**, 327–348 (2019). https://doi.org/10.3144/expresspolymlett.2019.28

[33] Li P., Ishiguro M.: Adsorption of anionic surfactant (sodium dodecyl sulfate) on silica. Soil science and plant nutrition, **62**, 223–229 (2016). https://doi.org/10.1080/00380768.2016.1191969

[34] Aguilar-Bolados H., Brasero J., López-Manchado M. A., Yazdani-Pedram M.: High performance natural rubber/thermally reduced graphite oxide nanocomposites by latex technology. Composites Part B: Engineering, **67**, 449–454 (2014). https://doi.org/10.1016/j.compositesb.2014.08.010

[35] Zhan Y., Liu G., Xia H., Yan N.: Natural rubber/carbon black/carbon nanotubes composites prepared through ultrasonic assisted latex mixing process. Plastics, Rubber and Composites, **40**, 32–39 (2011). https://doi.org/10.1179/174328911X12940139029284

[36] Wei L., Fu X., Luo M., Xie Z., Huang C., Zhou J., Zhu Y., Huang G., Wu J.: Synergistic effect of CB and GO/CNT hybrid fillers on the mechanical properties and fatigue behavior of NR composites. RSC Advances, **8**, 10573–10581 (2018). https://doi.org/10.1039/C7RA12830D

[37] Ahankari S. S., Kar K. K.: Hysteresis measurements and dynamic mechanical characterization of functionally graded natural rubber–carbon black composites. Polymer Engineering and Science, **50**, 871–877 (2010). https://doi.org/10.1002/pen.21601

[38] Alamusi, Hu N., Fukunaga H., Atobe S., Liu Y., Li J.: Piezoresistive strain sensors made from carbon nanotubes based polymer nanocomposites. Sensors, **11**, 10691–10723 (2011). https://doi.org/10.3390/s111110691

[39] Ilinykh I., Muratov D. S., Gorshkov N., Burmistrov I., Kuznetsov D., Yakovlev E.: Influence of MWCNT concentration on electrical conductivity of ethylene-1-octene composites. Nanomechanics Science and Technology, **5**, 223–228 (2014). https://doi.org/10.1615/NanomechanicsSciTechnolIntJ.v5.i3.60

[40] Krainoi A., Johns J., Kalkornsurapranee E., Nakaramontri Y.: Carbon nanotubes reinforced natural rubber composites. in 'Carbon nanotubes' (eds.: Ghosh P. K., Datta K., Rushi A. D.) IntechOpen, Rijeka, 47–68 (2021). https://doi.org/10.5772/intechopen.95913

[41] Thomas P. S., Abdullateef A. A., Al-Harthi M. A., Atieh M. A., De S., Rahaman M., Chaki T., Khastgir D., Bandyopadhyay S.: Electrical properties of natural rubber nanocomposites: Effect of 1-octadecanol functionalization of carbon nanotubes. Journal of Materials Science, **47**, 3344–3349 (2012). https://doi.org/10.1007/s10853-011-6174-4

[42] Yoshikawa S., Ota T., Newnham R., Amin A.: Piezoresistivity in polymer-ceramic composites. Journal of the American Ceramic Society, **73**, 263–267 (1990). https://doi.org/10.1111/j.1151-2916.1990.tb06504.x

[43] Zheng Y., Li Y., Dai K., Wang Y., Zheng G., Liu C., Shen C.: A highly stretchable and stable strain sensor based on hybrid carbon nanofillers/polydimethylsiloxane conductive composites for large human motions monitoring. Composites Science and Technology, **156**, 276–286 (2018). https://doi.org/10.1016/j.compscitech.2018.01.019